Biointerface Research in Applied Chemistry
Platinum Open Access Journal (ISSN: 2069-5837)

Article
Volume 12, Issue 6, 2022, 7147 - 7158
https://doi.org/10.33263/BRIAC126.71477158

Synthesis, Characterization of $ZrO_2:Tb^{3+}$ (1-9 mol %) Nanophosphors for Blue Lighting Applications and Antibacterial Property

H. J. Amith Yadav [1,*], B. Eraiah [2], Muttanagoud N. Kalasad [1,*], M. Thippeswamy [3], V.Rajasreelatha [4]

1 Department of Studies in Physics, Davangere University, Davangere577007, India amithyadavhj@gmail.com (H.J.A.Y); mnkalasad@gmail.com (M.N.K);
2 Department of Physics, Bangalore University, Bangalore 560056, India; eraiah@rediffmail.com (B.E.);
3 Department of Studies in Botany, Davangere University, Davangere 577007, India thippeswamym@davangereuniversity.ac.in (M.T.);
4 Department of Biochemistry, Indian Institute of Science, Bangalore-560012, India 4; vrajasreelatha@gmail.com (V.R.);
* Correspondence: amithyadavhj@gmail.com (H.J.A.Y); mnkalasad@gmail.com (M.N.K);
Scopus Author ID 57021721300 (H.J.A.Y); 23988904800 (M.N.K);
Received: 2.09.2021; Revised: 20.10.2021; Accepted: 24.10.2021; Published: 24.11.2021

Abstract: This paper reports the structural, morphological, and antibacterial studies of $ZrO_2:Tb^{3+}$ nanophosphors (NPs). The $ZrO_2:Tb^{3+}$ NPs were synthesized by hydrothermal route using Amylamine as surfactant. $ZrO_2:Tb^{3+}$ nanophosphors was characterized by Powder X-ray Diffraction(PXRD), Scanning Electron Microscope (SEM),Diffuse reflectance spectroscopy (DRS), Photoluminescence(PL), Raman spectra, Fourier Transform Infrared radiation(FTIR) and Transmission Electron Microscope(TEM). PXRD analysis shows better crystallinity, cubic in-phase and good homogeneity of the synthesized phosphors were confirmed. When the Tb^{3+} concentration varies, we obtain blue emissions from $ZrO_2:Tb^{3+}$ NPs. $ZrO_2:Tb^{3+}$ NPs have a promising approach to blue light sources in the display application. SEM images show that $ZrO_2:Tb^{3+}$ nanophosphors have good morphology with a nonporous structure. TEM and SAED pattern confirms that $ZrO_2:Tb^{3+}$ nanophosphors are crystalline in nature. $ZrO_2:Tb^{3+}$ (9mol %) nanophosphors possessed a good antibacterial ability.

Keywords: nanophosphors; Raman spectra; hydrothermal technique; Rietveld refinement; surfactant.

1. Introduction

The significance of nanophosphors in the field of research has been hugely developed because of their optical property [1]. They were broadly utilized in display applications [2], luminescent security ink [3], solar cell applications[4], bioimaging[5],photonic applications[6], etc. Zirconia assumes an essential job in the field of catalyst because it has a high surface-to-volume ratio[7]. Zirconium Oxide is used in the treatment of organic pollutants[8], biomedical applications[9], neuroscience[10], mammary cancer imaging in mice[11]. ZrO_2 is nanophosphors exists in three crystalline phases at different temperature, i.e., cubic phase(>2640K), tetragonal phase(1440-2640K) and monoclinic phase(<1440K) [12]. To date, different methodologies have been used to synthesize the ZrO_2 nanophosphors, i.e., co-precipitation method [13], Microwave method [14], Sol-gel method [15], spray pyrolysis deposition [16], and combustion method[17], etc.

In this work, we are using the hydrothermal method to synthesize $ZrO_2:Tb^{3+}$ nanophosphors because of high reaction rates and control over crystalline size and shape [10]. Amylamine as a surfactant is used to synthesize $ZrO_2:Tb^{3+}$ nanophosphors, and also it helps in stabilizing the nanoparticles[18]. The effect of Tb doping on the antibacterial properties of the Tb-doped ZrO_2 nanoparticles was investigated.

White light-emitting diodes are new-age lighting frameworks due to their novel properties like high productivity, low power utilization, and not containing harmful materials like mercury. Tb^{3+}doped materials show blue emission and green emission. As a result lot of attention must be put on Tb^{3+} doped hosts for their conceivable application in WLEDs. Moreover, there is a developing interest in growing profoundly effective rare earth (RE) doped ZrO_2 nanophosphors to deliver WLEDs.

Zirconia particles and Zirconia-based compounds are profoundly poisonous to microorganisms because of their mechanical properties and biocompatibility. Zirconia-based nonmaterial as antibacterial part have been utilized in dental earthenware and their covering of clinical gadgets [19]. The present investigation is committed to studying the phase, energy band gap, morphology, and antibacterial activity [20] of $ZrO_2:Tb^{3+}$ nanophosphors. The novelty of the present work is the ability to regulate the blue color by changing the concentration of Tb^{3+}.

2. Materials and Methods

2.1. Synthesis.

Hydrothermal method is used to synthesis $ZrO_2:Tb^{3+}$ nanophosphors. Zirconium (IV) propoxideand terbium (III) nitrate pentahydrate is a precursor required for synthesis. Zirconium (IV) propoxide was dissolved in methoxy ethanol and stirred continuously for 4 hrs. The nitrate salt of Terbium (III) Nitrate Pentahydrate is dissolved in double distilled water to get the aqueous solution of Terbium nitrate [21]. The reaction mixture is constantly stirred for 20min on a magnetic stirrer and mixed in zirconium propoxide solution and the reaction mixture's pH solution. Then, at that time, the pH of the solution was acclimatized to 10 by the addition of 2M of NaOH solution under constant stirring. The resulting reaction mixture was added to a Teflon-lined stainless steel autoclave of 300 ml, filled with 80% solvent constituted by 60 % double distilled water and 20% Amylamine, which acted as a surfactant [22]. Autoclave acts as temperature gradient was kept in a hot air oven at 150^o C for 24 h reaction time. Then the reaction mixture was centrifuged and dried in a vacuum oven at 80°C for 6 hrs. Then, at this point, the autoclave was placed in a hot air furnace at 150^o C for 24 hours (optimized time). After hydrothermal treatment, REMI R-24 Centrifuge was used to centrifuge the arrangement Machine at 5500 rpm for 10 min and washed with twofold refined water to remove salt, which is delivered during the reaction. The centrifugation process was rehashed multiple times. Precipitation was dried in a vacuum oven at 80^{O}C for 6 hrs to remove water content. The final product was calcined at 600^{o}C for 4h[23].

2.2. Antibacterial activity.

To study the antibacterial properties, the materials used are $ZrO_2:Tb^{3+}$ (9mol%), Mueller–Hinton media, Petri plates, filter paper disc. From MTCC (Microbial Type Culture Collection) Chandigarh, India, following materials such as Two Gram-positive bacteria *Bacillus subtilis, Staphylococcus aureus,* and Two Gram-Negative bacteria *Escherichia coli,*

Salmonella typhi subcultured on nutrient Mueller-Hinton and incubated at 37°C. The bacterial suspensions were prepared by selecting a single colony and cultured in different test tubes containing nutrient media for 24 h at 37°C.

To identify the potentiality of all nanoparticles in different concentrations range from 0.0025 µg/mL to 0.015 µg//mL as antibacterial agent, the bacterial strains were inoculated in sterile test tubes containing M-H media for 24 h at 37 °C. The bacterial growth was measured at a wavelength of 600 nm using a spectrophotometer; the ZrO_2:Tb^{3+} (9mol%) culture showed less growth compared to other different doped concentrations of nanoparticles. The synthesized ZrO_2:Tb^{3+} (9mol%) nanoparticle was used for further characterization.

Mueller−Hinton agar plates were prepared, and the entire surface of the plate inoculum was evenly spread. Before applying nanoparticles to the disc, let the plate dry. Different concentrations of nanoparticles were used for the antibacterial activity.

The agar plate was divided into six sections to understand the differential antibacterial activity by filter paper disc diffusion method using the suspension of bacteria spread on a Mueller−Hinton agar plate.

The different concentrations of synthesized ZrO_2:Tb^{3+} (9mol%) nanoparticles were dissolved in sterile water and briefly sonicated.

On the surface of the filter paper disc, each sample of the nanoparticles was loaded. The antimicrobial activity was surveyed by assessing the zone of inhibition against the test organisms with a caliper. The antimicrobial test for every bacterium made three steps [24].

3. Results and Discussion

3.1. Powder X-ray diffraction and Rietveld refinement.

The PXRD patterns of ZrO_2:Tb^{3+} (1−9mol %)NPs are shown in fig.1. The PXRD patterns show the cubic phase structure, and peaks are matched with standard JCPDS card No. 899069 for confirmation [25].

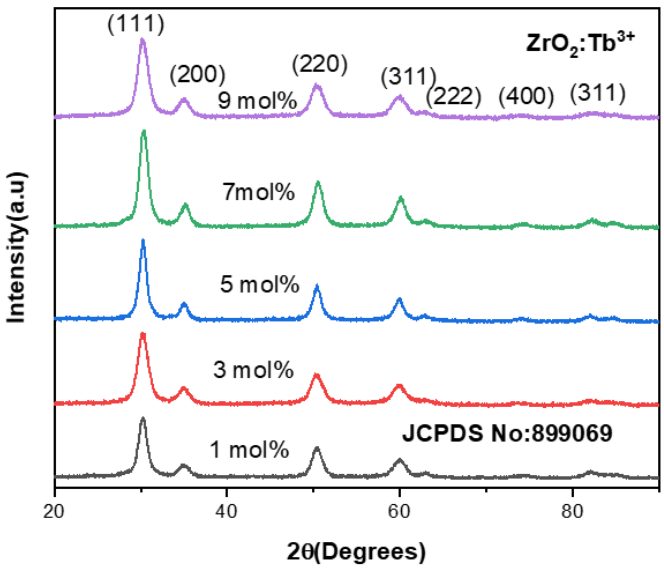

Figure 1. PXRD patterns of ZrO_2:Tb^{3+} (1−9mol %) nanophosphor.

Fig 2 shows Rietveld refinement of XRD patterns has been carried out using Fullprof suite software to provide proof for cubic phase with space group Fm-3m, which is in good agreement with JCPDS No. 899069. Cations have been set to (0, 0, 0) wyckoff from:4a, and O

atoms have been set to 1/4, 1/4, 1/4 wyckoff position:8c.In Rietveld refinement [26], technique intensity extraction occurred using the least square method and different experimental methods, and the sample-dependent peak broadening effect is studied. Here iterative refinement procedure is essential to obtain the potential fit between calculated and observed crystal structure. Parameters such as atomic positions, anisotropic displacement parameter, occupations, chemical binding, and geometry characteristics of the molecule in the structure model were modified using the least square methods [22].

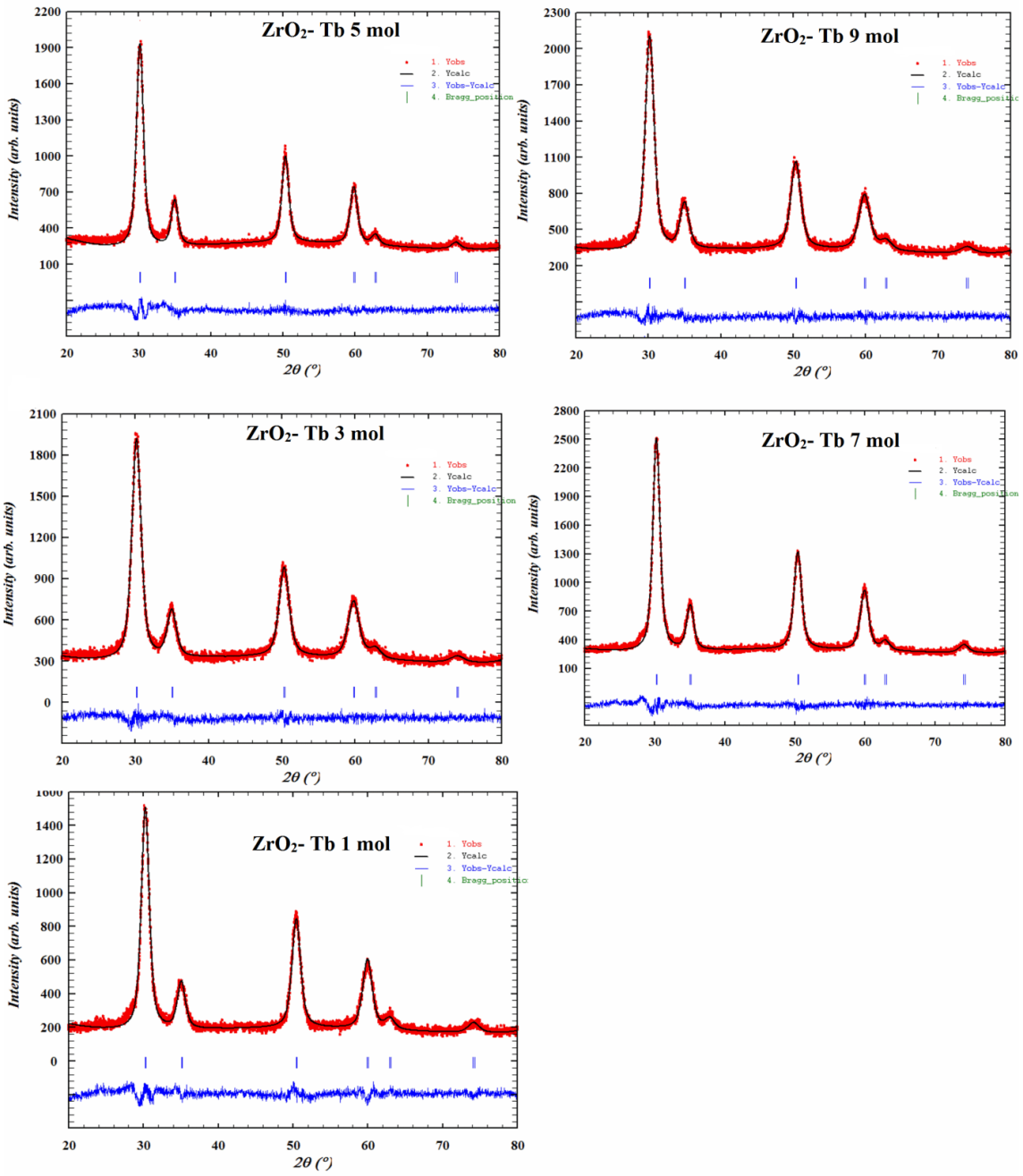

Figure 2. Rietveld refinement of ZrO_2:Tb^{3+} (1−9mol %) nanophosphors.

VESTA (Visualization for Electronic and Structural Analysis) software is used to study structural determination in crystallography, i.e., the volume of the unit cell, bond length, and angle [27]. Structural distortion in terms of bond length (R) and bond angle concerning dopant are tabulated in Table 1. There is no significant variation in the lattice parameters and volume

of the unit cell with increasing Tb^{3+} concentration [28]. Figure 3 shows the 3D structure of zirconia.

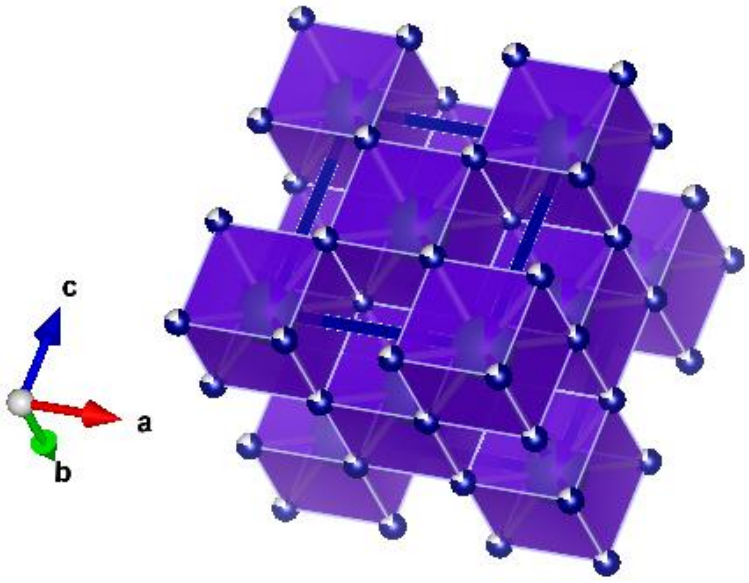

Figure 3. 3D structure of Zirconia.

Table 1. Rietveld Refinement Factors of ZrO_2:Tb^{3+}(1−9mol %) nanophosphors.

Sr. No.	Sample	Goodness of fit (χ^2)	Lattice Parameter (Å)	Volume of Unit Cell (Å^3)	Zr-O(Å)	Zr-Zr(Å)	Electron Density around Zr	Oxygen Occupancy
1	ZrO_2:Tb^{3+} (1 mol %)	1.49	5.1161	133.911	2.2153	3.6176	48.7022	1.8157
2	ZrO_2:Tb^{3+} (3 mol %)	1.04	5.1279	134.839	2.2204	3.6260	48.2895	1.7776
3	ZrO_2:Tb^{3+} (5 mol %)	1.86	5.1259	134.682	2.2196	3.6246	48.8062	1.6138
4	ZrO_2:Tb^{3+} (7 mol %)	1.39	5.1172	133.997	2.2158	3.6184	48.5176	1.7346
5	ZrO_2:Tb^{3+} (9 mol %)	1.06	5.1254	134.642	2.2194	3.6242	48.2535	1.6149

3.2. Scanning electron microscope.

Fig. 4(a-e) shows the SEM images of ZrO_2:Tb^{3+}nanophosphors. It is observed that the morphology is uniform and similar to ovoid-like morphology. It has no voids and is porous.

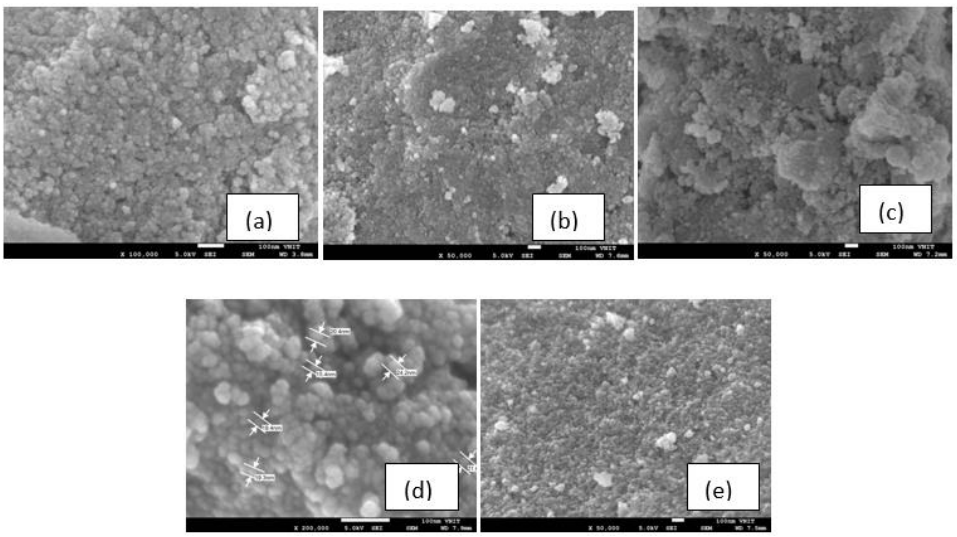

Figure 4. Scanning electron microscopy analysis of ZrO_2:Tb^{3+}nanophosphors.

3.3. Diffuse reflectance spectroscopy.

Fig 5 shows the energy band gaps of ZrO_2:Tb^{3+}(1-9mol%) nanophosphors. To calculate the bandgap of the NPs, Kubelka-Munk relation was used [29]. The bandgap of energy varies from 4.71–4.9 eV.

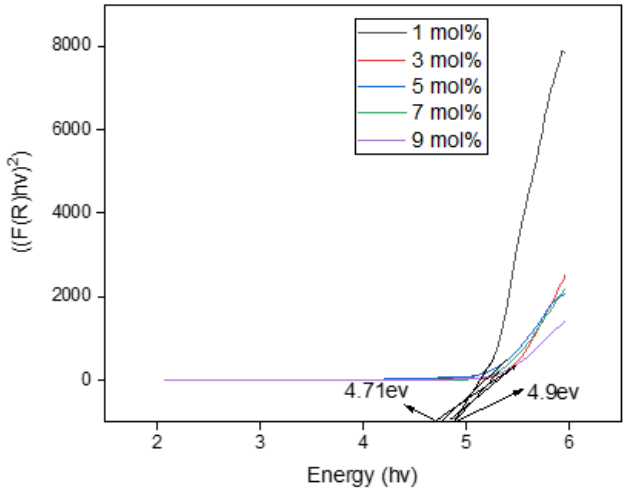

Figure5. Energy band gaps of ZrO_2: Tb^{3+} (1–9 mol %) nanophosphor.

3.4. Photoluminescence.

After excitation at 300 nm, emission spectrums were recorded for all nanophosphors, as shown in Fig. 6. The green emission above 480 nm was reported as a result of the advance of$^5D_4 \rightarrow {}^7F_J$ transition, while the transition of $^5D_3 \rightarrow {}^7F_J$ was responsible for the blue emission below 480 nm. In the present work, emission peaks at 466nm, 542nm because of $^5D_3 \rightarrow {}^7F_5$, $^5D_4 \rightarrow {}^7F_5$ transitions[1].

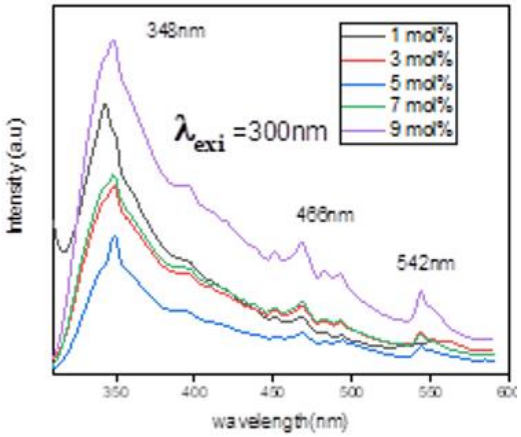

Figure 6. PL emission spectra of ZrO_2:Tb^{3+} (1–9 mol%) nanophosphor excited at 300 nm.

The luminescent emission color of ZrO_2:Tb^{3+} (1-9 mol%) NPs indicated by the 1931 chromaticity coordinates of the International Commission on Illumination (CIE). These coordinates represent the distinctive visible colors produced by the phosphors. The CIE chromaticity coordinates for the optimized sample were calculated from the emission spectra measured under 300 nm excitation wavelength, and the results are shown in Fig.7[30]. When the Tb^{3+} concentration varied, the color coordinates in the chromaticity diagram ranged from deep blue to light blue[31]. Table 2 shows the variation of Commission International de

L'Eclairage (CIE) chromaticity coordinates of the ZrO_2:Tb^{3+} (1–9 mol%) phosphors under excitation wavelength at 300 nm.

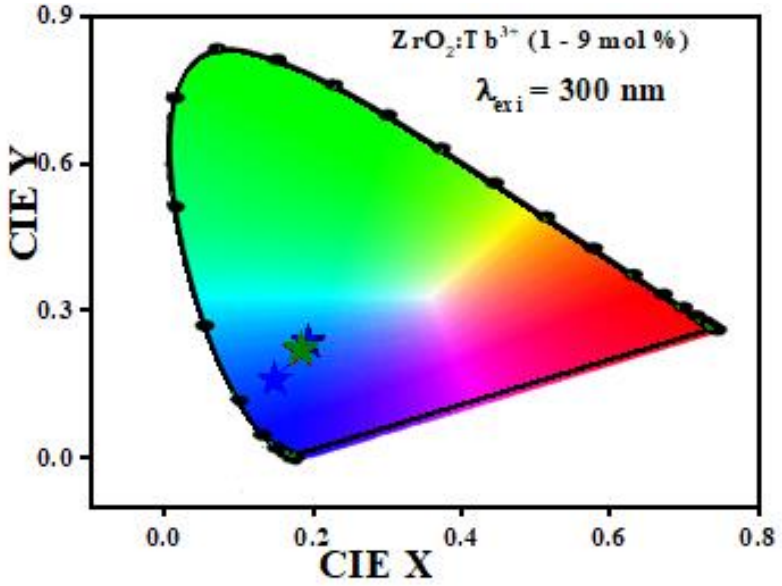

Figure 7. CIE chromaticity of ZrO_2:Tb^{3+} (1–9 mol%) nanophosphors.

Table 2. CIE chromaticity coordinates of the ZrO_2:Tb^{3+} (1–9 mol%) nanophosphors under excitation wavelength at 300 nm.

mol%	x	y
1	0.148172	0.159479
3	0.19355	0.235565
5	0.190875	0.239043
7	0.183765	0.218761
9	0.184044	0.220916

3.5. Raman spectra.

The Raman spectra of ZrO_2: Tb^{3+} (1-9 mol %) NPs recorded in the range of 530−1000 cm^{-1}areshown in Figure 8. From Figure 8, the peaks were observed at 548 cm^{-1} (A_{1g}), 563cm^{-1}(A_{1g})[25], and 651 cm^{-1} (T_{2g})[32].In Figure 8, the peaks correspond to the cube ZrO_2: Tb^{3+} (1-9 mol%) NPs.

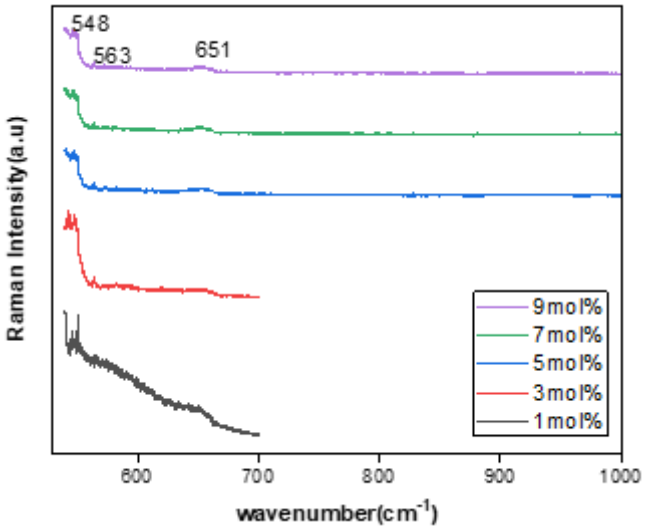

Figure 8. Raman spectra of the ZrO_2: Tb^{3+} (1-9 mol %) NPs.

3.6. Fourier Transform Infrared radiation.

Figure 9 shows the FTIR spectra of the ZrO_2:Tb^{3+} (1-9 mol %) Nanophosphors recorded in the range from 450 to 4500cm^{-1}. It gives information about the absolute OH content of the phosphors. The stretching frequencies of Zr – O bond is due to the band at 1133 cm^{-1}. The bending vibration of the OH group is due to 1424 cm^{-1}. The bonds at 3664 cm^{-1} due to stretching vibrations of absorbed water molecules in the form of OH group vibrations also show low absorbance [33]. The peak at 1715cm^{-1} is due to the characteristic of the vibration of OH groups. The characteristic of the vibration of OH groups is due to 1715cm^{-1}[34].

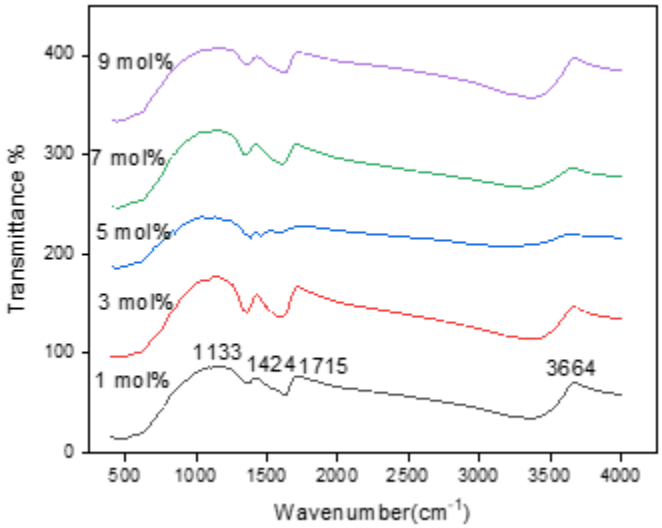

Figure 9. FTIR spectra of the ZrO_2: Tb^{3+} (1-9 mol %) NPs.

3.6. Transmission electron microscope.

Fig 10 shows the TEM and SAED patterns of ZrO_2:Tb^{3+} (9mol %) nanophosphors. Tem images show particles are tightly packed. SAED pattern confirms crystalline structure.

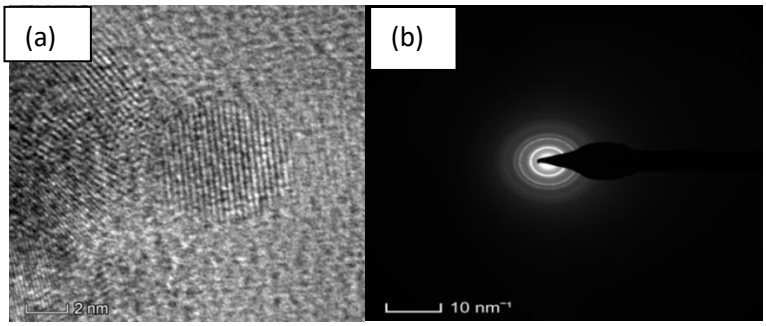

(a) **(b)**

Figure 10. (a) TEM and (b) SAED pattern of ZrO_2:Tb^{3+} (9 mol%) nanophosphors.

3.7. Antibacterial activity.

The filter paper disk diffusion assay was performed to test the inhibition zone of ZrO_2:Tb^{3+}(9mol%) NPs against human pathogenic Gram-positive *B. subtilis, S. aureus,* and Gram-negative *E coli, S typhi* bacteria. Here, the ZrO_2:Tb^{3+}(9mol%)NPs showed activity against all the tested bacteria at different concentrations. The data show that the inhibition zone diameter for synthesized ZrO_2:Tb^{3+}(9mol%)NPs gradually increased with increasing

concentration. The antibacterial activities were tested against four bacteria species which include two Gram-positive bacteria: *B. subtilis, S. aureus* inhibition showed higher than the other two Gram-negative bacteria: *E. coli, S typhi.*

Table 3 shows the antibacterial activity studies. Increased inhibition of the zone leads to the destruction of bacterial cells due to the increased formation of reactive oxygen species (ROS) [35]. These elevated ROS disrupts the bacterial cell membrane by lipid peroxidation and lead to a high level of membrane leakage results in bacterial death with increasing concentration of nanoparticles [36]. In the present study, the binding of ZrO_2:Tb^{3+}(9mol%) NPs to bacteria depends on the surface area available for interaction with the cell surface, which penetrates and changes take place in its cell membrane morphology and physiology. The ROS modulates cell function, which leads to DNA damage, protein denaturation, turnover of lipids induces oxidative stress. This will enable to generate ROS through different biochemical pathways. The DNA damage is due to induced ROS [37].

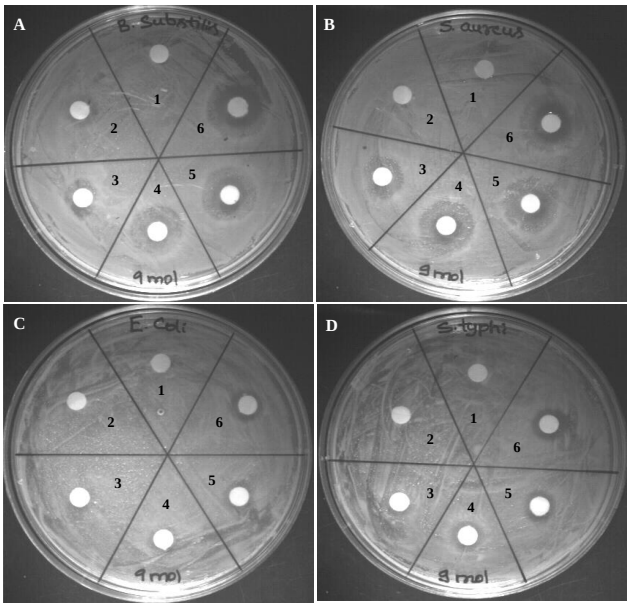

Figure 11. Antibacterial effects of ZrO_2:Tb^{3+}(9mol%). 1. Control, 2. 0.0025 µg/mL, 3. 0.005 µg/mL, 4. 0.0075 µg/mL, 5. 0. 01 µg/mL and 6. 0.015 µg/mL.

Table 3. Antibacterial activity of ZrO_2:Tb^{3+}(9mol%) nanophosphors on Gram-positive; *Bacillus subtilis*, *Staphylococcus aureus*, and Gram-negative; *Escherichia coli*, *Salmonella typhi*.

ZrO_2:Tb^{3+} (9mol%)(µg)	**Gram-positive bacteria**		**Gram-negative bacteria**	
	Zone of inhibition in mm			
	B. subtilis	***S. aureus***	***E. coli***	***S. typhi***
Control	0.00	0.0	0.00	0.00
25	0.13	0.14	0.00	0.00
50	0.24	0.27	0.00	0.11
75	0.35	0.36	0.21	0.23
100	0.43	0.45	0.33	0.32
150	0.52	0.58	0.42	0.41

4. Conclusions

Tb doped zirconium oxide NPs were synthesized by Hydrothermal synthesis route with Amylamineas surfactant. PXRD image reveals it is cubic in shape. Retevield refinement confirms cubic in phase; Raman patterns support PXRD patterns. DRS pattern shows bandgap varies from 4.17-4.9ev. SEM and TEM provide morphology of ZrO_2:Tb^{3+} NPs. SAED pattern confirms crystalline in phase. The ZrO_2:Tb^{3+} NPs belong to one kind of novel optical material

as a promising future candidate for strong blue emission and have drawn an increasing amount of attention. In the antibacterial activity of ZrO_2:Tb^{3+}(9mol%), NPs were more effective against selected Gram-positive bacteria than on selected Gram-negative bacteria.

Funding

This research received no external funding.

Acknowledgments

The authors are grateful to Prof. Smita A Acharya, Rashtrasant Tukadoji Maharaj Nagpur University, IITM SAIF, INUP-IISc, and CeNSE, Bangalore, for the characterization of the compound.

Conflicts of Interest

The authors declare no conflict of interest.

References

1. Vidya, Y.S.; Gurushantha, K.; Nagabhushana, H.; Sharma, S.C.; Anantharaju, K.S.; Shivakumara, C.; Suresh, D.; Nagaswarupa, H.P.; Prashantha, S.C.; Anilkumar, M.R. Phase transformation of ZrO_2:Tb^{3+} nanophosphor: Color tunable photoluminescence and photocatalytic activities. *Journal of Alloys and Compounds* **2015**, *622*, 86-96,https://doi.org/10.1016/j.jallcom.2014.10.024.
2. Kumar, A.N.; Jnaneshwara, D.M.; Nagabhushana, H.; Pratapkumar, C.; Ravikumar, C.R.; Kumar, M.R.A.; Shekhar, T.R.S.; Prashantha, S.C. Photoluminescence, photocatalytic and electrochemical performance of $La_{10}Si_6O_{27}$:Sm^{3+} nanophosphor: It's applications in display, photocatalytic and electrochemical sensor. *Applied Surface Science Advances* **2021**, *4*,https://doi.org/10.1016/j.apsadv.2021.100070.
3. Sandhyarani, A.; Kokila, M.K.; Darshan, G.P.; Nagabhushana, H.; Sharma, S.C.; Premkumar, H.B.; Prasad B, D. Fabrication of flux supported $SrTiO_3$:Eu^{3+} fluorescent powders: New prospective of dual mode, ink-free data security applications. *Journal of Science: Advanced Materials and Devices* **2021**, *6*, 92-99, https://doi.org/10.1016/j.jsamd.2020.11.004.
4. Michaels, H.; Benesperi, I.; Freitag, M. Challenges and prospects of ambient hybrid solar cell applications. *Chemical Science* **2021**, *12*, 5002-5015, https://doi.org/10.1039/D0SC06477G.
5. Geppert, M.; Himly, M. Iron Oxide Nanoparticles in Bioimaging–An Immune Perspective. *Frontiers in Immunology* **2021**, *12*, https://dx.doi.org/10.3389%2Ffimmu.2021.688927.
6. Manoli, A.; Papagiorgis, P.; Sergides, M.; Bernasconi, C.; Athanasiou, M.; Pozov, S.; Choulis, S.A.; Bodnarchuk, M.I.; Kovalenko, M.V.; Othonos, A.; Itskos, G. Surface Functionalization of $CsPbBr_3$ Nanocrystals for Photonic Applications. *ACS Applied Nano Materials* **2021**, *4*, 5084-5097, https://doi.org/10.1021/acsanm.1c00558.
7. Renuka, L.; Anantharaju, K.S.; Sharma, S.C.; Nagabhushana, H.; Vidya, Y.S.; Nagaswarupa, H.P.; Prashantha, S.C. A comparative study on the structural, optical, electrochemical and photocatalytic properties of ZrO_2 nanooxide synthesized by different routes. *Journal of Alloys and Compounds* **2017**, *695*, 382-395, http://dx.doi.org/10.1016%2Fj.jallcom.2016.10.126.
8. Singh, H.; Sunaina; Yadav, K.K.; Bajpai, V.K.; Jha, M. Tuning the bandgap of m-ZrO_2 by incorporation of copper nanoparticles into visible region for the treatment of organic pollutants. *Materials Research Bulletin* **2020**, *123*, https://doi.org/10.1016/j.materresbull.2019.110698.
9. Barabás, R.; Fort, C.I.; Turdean, G.L.; Bizo, L. Influence of HAP on the Morpho-Structural Properties and Corrosion Resistance of ZrO_2-Based Composites for Biomedical Applications. *Crystals* **2021**, *11*,https://doi.org/10.3390/cryst11020202.
10. Słońska, A.; Kaszewski, J.; Wolska-Kornio, E.; Witkowski, B.; Wachnicki, Ł.; Mijowska, E.; Karakitsou, V.; Gajewski, Z.; Godlewski, M.; Godlewski, M.M. Luminescent properties of ZrO_2:Tb nanoparticles for applications in neuroscience. *Optical Materials* **2016**, *59*, 96-102, https://doi.org/10.1016/j.optmat.2016.01.027.
11. Kaszewski, Jarosław, Emanuel Borgstrom, Bartłomiej S. Witkowski, Łukasz Wachnicki, Paula Kiełbik, Anna Slonska, Malgorzata A. Domino et al.Terbium content affects the luminescence properties of ZrO_2: Tb nanoparticles for mammary cancer imaging in mice, *Opt. Mater*, **2017**, 74, 16-26, https://doi.org/10.1016/j.optmat.2017.04.044.

12. Kurrey, U.; Brahme, N.; Bisen, D.P. Optical properties of rare earth (Ce) and transition metal (Ti) doped ZrO_2 phosphors. *IOP Conference Series: Materials Science and Engineering* **2021**, *1120*, https://doi.org/10.1088/1757-899X/1120/1/012002.
13. Ahmed, W.; Iqbal, J. Effect of Ni doping on structural, optical and magnetic characteristics of ZrO_2 nanoparticles with efficient visible light driven photocatalytic activity. *Ceramics International* **2021**, *47*, 24895-24905,https://doi.org/10.1016/j.ceramint.2021.05.216.
14. Sanaullah, I.; Imran, M.; Riaz, S.; Amin, T.; Khan, I.U.; Zahoor, R.; Shahid, A.; Naseem, S. Microwave assisted synthesis of Fe_3O_4 stabilized ZrO_2 nanoparticles – Free radical scavenging, radiolabeling and biodistribution in rabbits. *Life Sciences* **2021**, *271*,https://doi.org/10.1016/j.lfs.2021.119070.
15. Tabassum, N.; Kumar, D.; Verma, D.; Bohara, R.A.; Singh, M.P. Zirconium oxide (ZrO_2) nanoparticles from antibacterial activity to cytotoxicity: A next-generation of multifunctional nanoparticles. *Materials Today Communications* **2021**, *26*,https://doi.org/10.1016/j.mtcomm.2021.102156.
16. Habubi, N.F.; Abdulmunem, O.M.; Shaban, Z.M.; Agool, I.R.; Dawood, M.O.; Chiad, S.S. Effect of Cu doping ZrO_2 Thin films on physical properties grown by spray pyrolysis deposition. *IOP Conference Series: Earth and Environmental Science* **2021**, *790*,https://doi.org/10.1088/1755-1315/790/1/012078.
17. Ali, A.A.; Shama, S.A.; Amin, A.S.; El-Sayed, S.R. Synthesis and characterization of ZrO_2/CeO_2 nanocomposites for efficient removal of Acid Green 1 dye from aqueous solution. *Materials Science and Engineering: B* **2021**, *269*,https://doi.org/10.1016/j.mseb.2021.115167.
18. Sen, F.; Karatas, Y.; Gulcan, M.; Zahmakiran, M. Amylamine stabilized platinum(0) nanoparticles: active and reusable nanocatalyst in the room temperature dehydrogenation of dimethylamine-borane. *RSC Advances* **2014**, *4*, 1526-1531,https://doi.org/10.1039/C3RA43701A.
19. Alturki, A.M. Morphological, structural, microstructural and antibacterial features of silver-doped zirconia/hydroxyapatite for biomedical applications. *Applied Physics A* **2021**, *127*,1-11, https://doi.org/10.1007/s00339-021-04565-y.
20. Elangovan, M.; Dhayalan, R.; Krishnan, R. Green Synthesis of Silver Nanoparticles Using Flower Extract of Hemigraphis colorata as Reducing Agent and its Biological Activity. *Lett.Appl.NanoBioScience***2021,** *10*,2646–2654,https://doi.org/10.33263/LIANBS104.26462654.
21. Gupta, M.; Shirbhate, S.; Ojha, P.; Acharya, S. Processing and conductivity behavior of La, Sm, Fe singly and doubly doped ceria: As electrolytes for IT-SOFCs. *Solid State Ionics* **2018**, *320*, 199-209, https://doi.org/10.1016/j.ssi.2018.03.005.
22. Shirbhate, S.C.; Singh, K.; Acharya, S.A.; Yadav, A.K. Review on local structural properties of ceria-based electrolytes for IT-SOFC. *Ionics* **2017**, *23*, 1049-1057,https://doi.org/10.1007/s11581-016-1893-9.
23. Bhongale, K.; Shirbhate, S.; Acharya, S. Effect of sintering temperature on structural and electrical properties of co-doped ceria based electrolyte material for IT-SOFCs. *AIP Conference Proceedings* **2020**, *2220*,https://doi.org/10.1063/5.0002158.
24. Precious Ayanwale, A.; Reyes-López, S.Y. ZrO_2–ZnO Nanoparticles as Antibacterial Agents. *ACS Omega* **2019**, *4*, 19216-19224,https://doi.org/10.1021/acsomega.9b02527.
25. Yadav, H.J.A.; Eraiah, B.; Nagabhushana, H.; Darshan, G.P.; Prasad, B.D.; Sharma, S.C.; Premkumar, H.B.; Anantharaju, K.S.; Vijayakumar, G.R. Facile Ultrasound Route To Prepare Micro/Nano Superstructures for Multifunctional Applications. *ACS Sustainable Chemistry & Engineering* **2017**, *5*, 2061-2074, https://doi.org/10.1021/acssuschemeng.6b01693.
26. Shirbhate, S.C.; Yadav, A.K.; Acharya, S.A. Extended x-ray absorption fine structure spectroscopy and x-ray absorption near edge spectroscopy study of aliovalent doped ceria to correlate local structural changes with oxygen vacancies clustering. *Applied Physics Letters* **2016**, *108*,https://doi.org/10.1063/1.4945098.
27. Darunkar, S.S.; Acharya, S.A. Efficient acetone sensor based on Ni-doped ZnO nanostructures prepared by spray pyrolysis technique. *AIP Conference Proceedings* **2018**, *1953*,https://doi.org/10.1063/1.5032987.
28. Ahemen, I.; Dejene, F.B. Luminescence and energy transfer mechanism in Eu3+/Tb3+-co-doped ZrO2 nanocrystal rods. *Journal of Nanoparticle Research* **2016**, *19*,https://doi.org/10.1007/s11051-016-3703-8.
29. Jamil, H.; Dildar, I.M.; Ilyas, U.; Hashmi, J.Z.; Shaukat, S.; Sarwar, M.N.; Khaleeq-ur-Rahman, M. Microstructural and Optical study of polycrystalline manganese oxide films using Kubelka-Munk function. *Thin Solid Films* **2021**, *732*,https://doi.org/10.1016/j.tsf.2021.138796.
30. Jisha, P.K.; Prashantha, S.C.; Nagabhushana, H. Luminescent properties of Tb doped gadolinium aluminate nanophosphors for display and forensic applications. *Journal of Science: Advanced Materials and Devices* **2017**, *2*, 437-444,https://doi.org/10.1016/j.jsamd.2017.10.001.
31. Kumar, V.; Ntwaeaborwa, O.M.; Holsa, J.; Motaung, D.E.; Swart, H.C. The role of oxygen and titanium related defects on the emission of TiO_2:Tb^{3+} nano-phosphor for blue lighting applications. *Optical Materials* **2015**, *46*, 510-516,https://doi.org/10.1016/j.optmat.2015.05.011.
32. Lovisa, L.X.; Andrés, J.; Gracia, L.; Li, M.S.; Paskocimas, C.A.; Bomio, M.R.D.; Araujo, V.D.; Longo, E.; Motta, F.V. Photoluminescent properties of ZrO_2: Tm^{3+}, Tb^{3+}, Eu^{3+} powders—A combined experimental and theoretical study. *Journal of Alloys and Compounds* **2017**, *695*, 3094-3103, https://doi.org/10.1016/j.jallcom.2016.11.341.

33. Ahemen, I.; Dejene, F.B.; Botha, R. Strong green-light emitting Tb3+ doped tetragonal ZrO2 nanophosphors stabilized by Ba2+ ions. *Journal of Luminescence* **2018**, *201*, 303-313, https://doi.org/10.1016/j.jlumin.2018.05.003.
34. Di, W.; Wang, X.; Chen, B.; Lu, S.; Zhao, X. Effect of OH- on the Luminescent Efficiency and Lifetime of Tb^{3+}-Doped Yttrium Orthophosphate Synthesized by Solution Precipitation. *The Journal of Physical Chemistry B* **2005**, *109*, 13154-13158,https://doi.org/10.1021/jp051894i.
35. Panda,B.S.A. Review on Synthesis of Silver Nanoparticles and their Biomedical Applications. *Lett.Appl.NanoBioScience***2022**,11,3218–3231.
36. Amith Yadav, H.J.; Eraiah, B.; Nagabhushana, H.; Daruka Prasad, B.; Basavaraj, R.B.; Sateesh, M.K.; Shabaaz Begum, J.P.; Darshan, G.P.; Vijayakumar, G.R. Broad spectral inhibitory effects of pale green zinc oxide nanophosphor on bacterial and fungal pathogens. *Arabian Journal of Chemistry* **2018**, *11*, 324-342, https://doi.org/10.1016/j.arabjc.2017.12.012.
37. Fathima, J.B.; Pugazhendhi, A.; Venis, R. Synthesis and characterization of ZrO_2 nanoparticles-antimicrobial activity and their prospective role in dental care. *Microbial Pathogenesis* **2017**, *110*, 245-251,https://doi.org/10.1016/j.micpath.2017.06.039.